Compact Printed Diversity Antenna for LTE700/GSM1700/1800/UMTS/Wi-Fi/Bluetooth/LTE2300/2500 Applications for Slim Mobile Handsets

Hari S. Singh, Gaurav K. Pandey, Pradutt K. Bharti, and Manoj K. Meshram[*]

Abstract—A planar, printed multiple-input multiple-output (MIMO) antenna for slim mobile handset is presented. The dual-antenna system, comprises two symmetric antenna elements, is printed on a printed circuit board (PCB) of mobile phone. Each antenna element consists of coupled-fed loop antenna. The loop antenna is formed by a quarter wavelength (at 762 MHz) meandered loop strip with end terminal short-circuited to the ground plane. A T-shaped protruded ground is deliberately designed to enhance the impedance matching and decoupled the two closely deposed antenna elements (distance between antenna elements are 0.03λ at 762 MHz). The integrity of the T-shaped decoupling structure and coupled-fed loop antenna array covers LTE700 (0.747 GHz–0.787 GHz) and WWAN (1.7 GHz–3.04 GHz) based on -6 dB reflection coefficient and achieves isolation between elements well below -10 dB over all the operating bands. The application platform is LTE700, GSM1700, GMS1800, UMTS, Wi-Fi, Bluetooth, LTE2300, and LTE2500 bands for the 2G/3G/4G mobile terminals. The effect of user proximity by considering the actual mobile environment is also studied in the form of total radiated power (TRP), specific absorption rate (SAR), diversity performances, and radiation performances. Finally, a prototype is fabricated and tested with network analyser. The measured results are found in good agreement with simulated ones.

1. INTRODUCTION

In recent years, long term evolution (LTE) technology is going to stand in the front line of fourth generation (4G) mobile communications. As one of the key techniques in LTE, multiple-input multiple-output (MIMO) technology attracts significant attention of the researchers. The MIMO and diversity systems are potential technologies for enhancing the performances such as system reliability, channel capacity, and data transmission speed. It is because the MIMO system supports multiple independent channels at both transmitting and receiving sides to offer improved capacity over single antenna topology without extra radiated power and spectrum bandwidth [1].

So in view of the above, researchers focuse on the LTE technology with MIMO implementation. Some studies have been carried out to achieve LTE band with MIMO antenna configuration [2–10]. To obtain LTE 13 band, a closely mounted PIFA in conjunction with a T-shaped common radiator is proposed [2]. But the overall volume of the PIFA is not favourable for slim mobile handset due to non-planar structure. In [3], LTE MIMO antenna is designed over ferrite substrate which causes the excitation of surface wave, leading to lower radiation efficiency and gain. The folded technique is applied to miniaturize the antenna element and to accomplish LTE band with small form factor [4, 5]. But the geometry of the antenna becomes non-planar, which is not suitable for the slim handset. In [6],

* Corresponding author: Manoj Kumar Meshram (mkmeshram.ece@iitbhu.ac.in).

The authors are with the Department of Electronics Engineering, Indian Institute of Technology (Banaras Hindu University), Varanasi 221005, India.

meandered line technique is used to achieve compactness of the antenna. But the thickness of the antenna reaches a certain height due to such applied technique, and the planar nature of the antenna is disturbed. A quad-band mobile handset antenna is presented for LTE700 MIMO application [7], but the whole antenna system deposes on the one side of the PCB board which makes a larger form factor, and the antenna is designed over a carrier which will bring difficulties during fabrication process.

Further, the LTE/WWAN band with multiple antenna configurations is reported in [8–11]. In [8–11], coupled-fed antennas are embedded to get lower and wide upper bands. But to make the compact structure, the antennas are folded at the edges of the strips which provide 3D geometry leading to difficult fabrication steps. The chip inductor is used in the design of antennas to minimize the physical length required for desired resonant modes, which produces losses as well as increase fabrication process. All the above constraints are strict to implement the antennas in modern day mobile handsets.

Somehow, multiple antennas within limited space of mobile phone have been implemented successfully. But mutual coupling between closely packed antenna elements is one of the key challenges. So, the most important recent issue is how to design compact MIMO antennas at lower frequency bands and how to obtain sufficient isolation and low envelope correlation coefficient (ECC) between closely placed antenna in portable MIMO-embedded devices. Some of the aspirant isolation techniques have been reported in [12–15] to enhance the isolation between antenna elements. Several kinds of decoupling techniques are readily available, such as neutralization line technique [12], etching slots [13], decoupling circuit [14], by exciting new resonant mode [15], which utilizes the edges of two PIFAs as well as another slot cut on the ground plane to form a half-wavelength U-shape slot in-between, and protruded ground plane [16, 17]. However, neutralization strip, etching slots usually need to introduce some complex well tuned metal structure, which leads to additional area consumption. Furthermore, decoupling circuit is often used for the single and narrowband decoupling, which is not so applicable to wideband decoupling. The excitation of new resonant mode cannot be utilized for a ground plane with arbitrary size and shape (e.g., that of a mobile phone) because it may not be possible to match the decoupling slots well enough in order to excite the mode successfully. The area taken by protruded ground plane in [15, 16] is large, e.g., space is not left for the speaker, microphone or other electronics components which can be set into the mobile handset near the antenna element.

In this paper, a small-size printed LTE/WWAN band decoupled MIMO antenna design is presented. The size of each planar coupled-fed loop antenna is $20.5 \times 24 \, \text{mm}^2$ over a mobile circuit board (PCB) of size $110 \times 60 \, \text{mm}^2$. A T-shaped protruded ground plane is used between two antenna elements to reduce the mutual coupling between antenna elements. Due to which, $3 \, \text{dB}$ isolation enhancement is observed over all the higher operating bands. The major components which provide the near-field electromagnetic interaction with antennas include a liquid crystal display (LCD), a battery, a dielectric frame, a speaker, a camera, a microphone, and buttons. Additionally, the proposed design takes into account the potential performance degrading interaction between an antenna system and a human head in close proximity. In the presence of human head phantom SAR is calculated according to the American standard (FCC) ($1.6 \, \text{W/kg}$ over $1 \, \text{g}$ tissue) and European standard ($2 \, \text{W/kg}$ over $10 \, \text{g}$ tissue). Both simulated and measured S-parameters and radiation patterns are reported. The results suggest that the proposed design has significant potential for current and future wireless devices, including multi-band MIMO antennas for smart slim mobile phones.

2. ANTENNA CONFIGURATION AND DESIGN

Figure 1(a) shows the front and rear views of the proposed MIMO antenna. It consists of two symmetrical planar antennas on front side (no ground plane on the rear side in this area) of a low cost FR4 substrate (thickness is $0.8 \, \text{mm}$) with dielectric constant $\varepsilon_r = 4.4$ and loss tangent $\tan \delta = 0.018$. Each array element is connected to a 50-Ω coaxial connector to excite the antenna, with points A_1 and A_2 serving as feed points and points B_1 and B_2 serving as PCB shorting points. The rear view of the proposed antenna consists of protruded T-shaped ground plane used to enhance the isolation as well as impedance matching at higher frequency bands. The detail of the T-shaped protruded ground plane is given in Figure 1(a). Two capacitively coupled-fed shorted loop antennas are closely mounted with the separation of $12 \, \text{mm}$ (0.03λ at $762 \, \text{MHz}$). The detailed dimensions of the proposed shorted loop antenna are shown in Figure 1(b). The fabrication of the prototype is done on T-Tech QC-5000 Micro-Milling
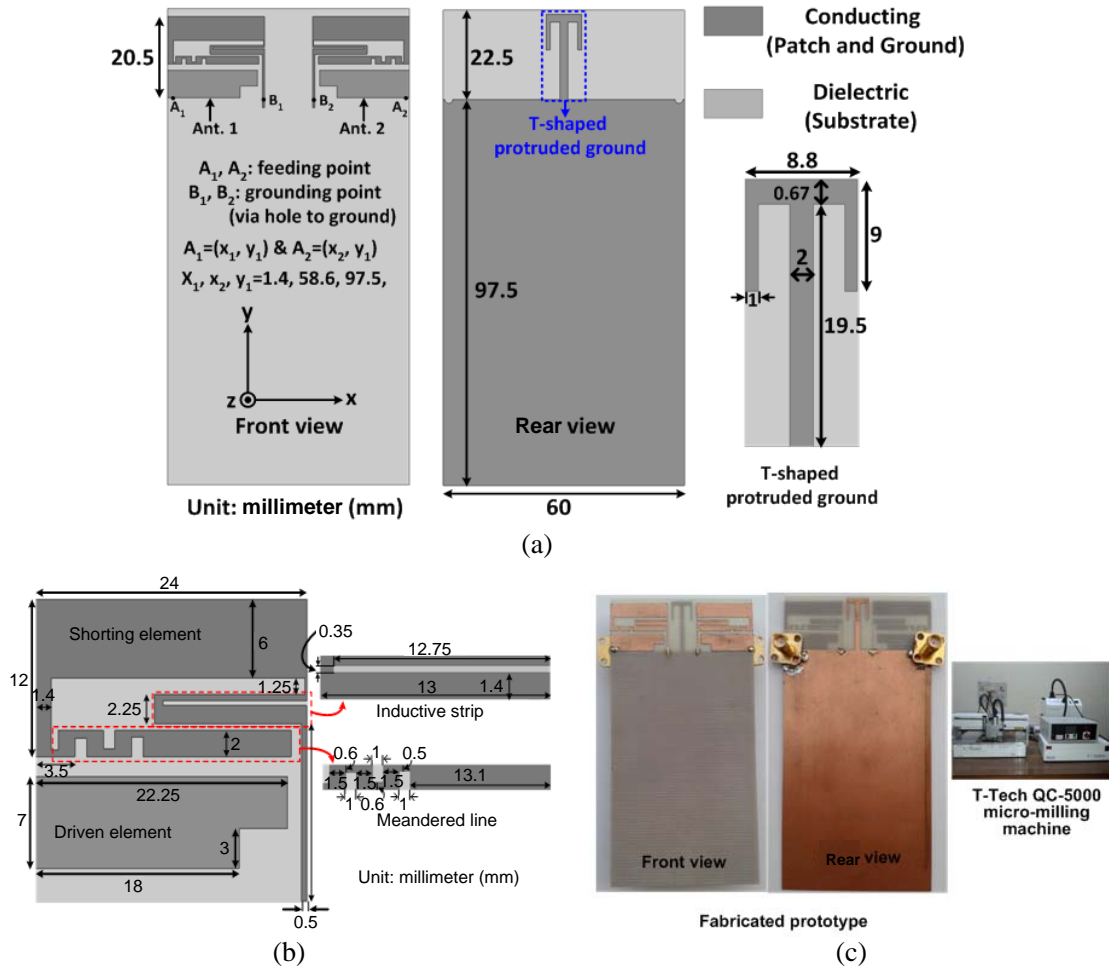
Figure 1. (a) Front and rear view of the proposed antenna, (b) detail dimensions of the single antenna element, and (c) fabricated prototype.
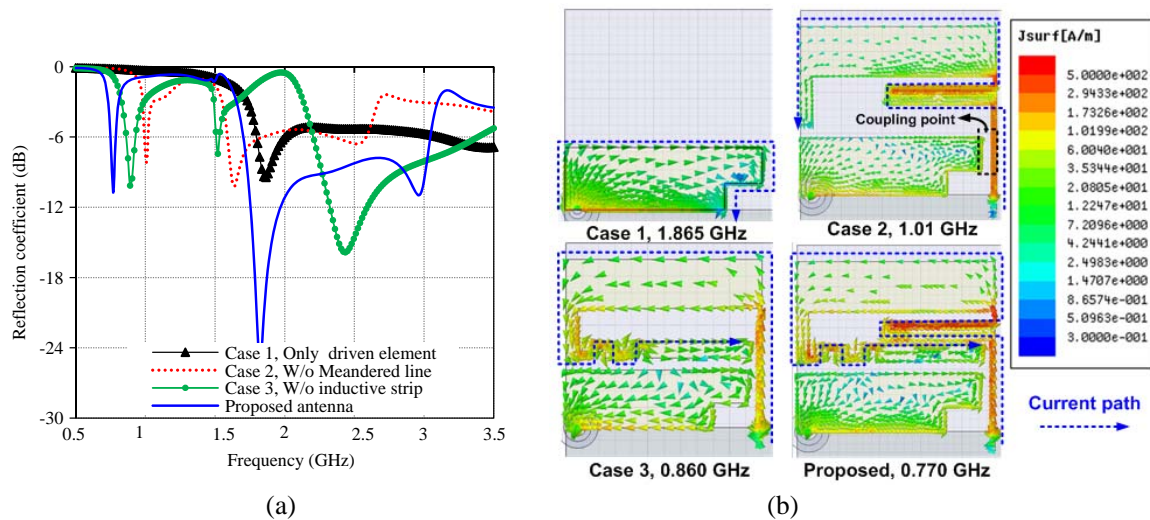
Figure 2. (a) Effect of different configurations on reflection coefficient, (b) surface current distribution for different cases.

Machine, shown in Figure 1(c).

To illustrate the design and mechanism of the proposed antenna, reflection coefficient and vector surface current distributions are shown in Figure 2. The evolution starts from the driven element and proceeds towards the proposed configuration to achieve the desired goal. Initially, driven element is designed to excite the main shorting strip loop antenna. The electrical length of the driven strip is $\lambda/4$ at 1.865 GHz ($\cong$ 40.5 mm), and the antenna resonates at 1.86 GHz corresponding to this electrical length as shown in Figure 2(a). Also vector surface current [Case 1, 1.865 GHz] starts travelling from feed point to outer boundary of the driven element (covers distance $\lambda/4$ at 1.865 GHz) which is responsible for 1.86 GHz resonance as shown in Figure 2(b). In order to achieve lower operating band and wideband operation at higher frequency band, a quarter wave strip with inductive strip is designed, and driven element is used as coupling feed, respectively. The current distribution [Case 2, 1.01 GHz] provides further explanation about the resonance mode at lower resonance frequency for Case 2. The coupling between the driven element and shorted loop strip provides wideband at higher frequency and due to flow of induced current from coupling point to end terminal of the loop provides the lower resonance frequency [dashed line shows current path in Figure 2(b)]. Further, to achieve lower resonance around LTE700 frequency band as well as to maintain compactness of the antenna, the idea is to add a meandered line structure at the end terminal of the shorting strip. Due to addition of the meandered line structure, the lower resonance shifts from 1.01 GHz to 0.861 GHz, but still LTE700 frequency band is not achieved. The occurrence of resonance at 0.861 GHz is due to the quarter wavelength of the meandered shorting strip. The current path [Case 3, 0.86 GHz] on the meandered shorted loop antenna starts flowing from coupling point to the end of meandered line which also confirms the resonance at 0.86 GHz. Finally, to get the desired goal, combination of meandered line and inductive strip is shorted with ground through via. With the combination of meandered line and inductive strip, total electrical length of the shorted loop antenna is increased, and resonance occurs at 0.767 GHz corresponding to the quarter wavelength of the shorting strip. After optimization of all the shape parameters, antenna resonates at 0.767 GHz, 1.813 GHz, and 2.95 GHz which covers the LTE700, GSM1700, GMS1800, UMTS, Wi-Fi, Bluetooth, LTE2300, and LTE2500 operating bands with below -10 dB isolation over all the operating bands.

3. RESULTS AND DISCUSSION

3.1. *S*-Parameters

All shape parameters of the proposed antenna are optimized using Ansoft's high frequency structure simulator (HFSS) [18], and before going for fabrication, optimized antenna is also simulated using computer simulation technology microwave studio (CST MWS) [19]. Further, CST MWS is used to evaluate the radiation performances and diversity performances. The fabricated prototype is measured
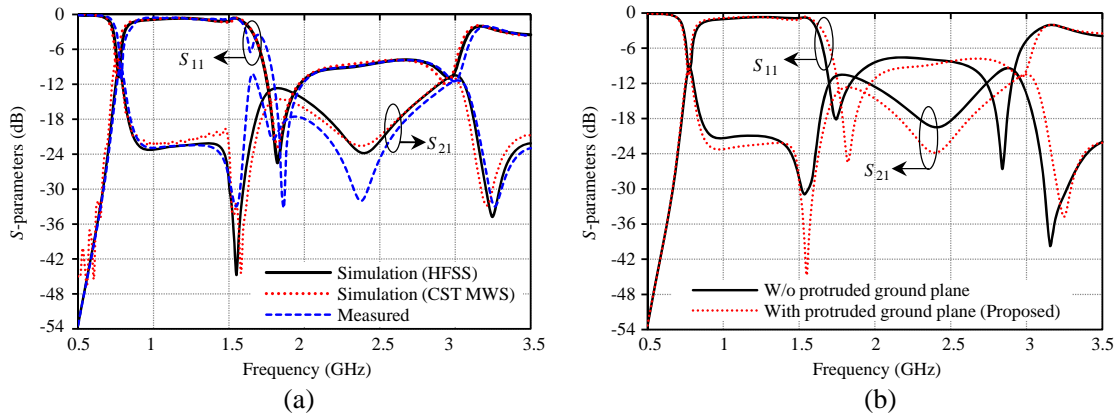
Figure 3. (a) Simulated and measured *S*-parameters, (b) effect of protruded ground plane on *S*-parameters.

by Anritsu VNA Master MS2038C (5 kHz–20 GHz). The simulated and measured S-parameters are shown in Figure 3(a). Some discrepancies between simulated and measured results are observed, which are due to manufacturing tolerances.

To study the effect of protruded ground plane, S-parameters are shown in Figure 3(b). It is observed that without the protruded ground plane, isolation at higher frequency side is less than -10 dB especially at two resonances, i.e., 1.68 GHz and 2.84 GHz. Apart from these two resonances, isolation is well below -10 dB. So it is required to enhance the isolation at higher frequency side especially at two higher resonances while the isolation at lower frequency side is maintained well below -10 dB. The isolation is significantly enhanced at higher frequency band for the proposed antenna with the T-shaped protruded ground plane, and improvement in impedance matching is also observed at higher frequency band. The effect of the protruded ground plane plays a significant role in isolation enhancement at higher frequency whereas insignificant role at lower frequency. This is because of the length of the protruded ground (T-shaped) is $\lambda/4$ which is corresponding to the higher frequency, i.e., 2.45 GHz.

In order to consider a real scenario, a typical hand-held geometric model is shown in Figure 4(a), which is based on near-field environments. The mobile environment comprises large size touch screen LCD ($72 \times 53 \times 2$ mm^3), battery ($64 \times 46 \times 3$ mm^3), camera (diameter is 17 mm and thickness 6.5 mm), and speaker ($18 \times 1 \times 1.8$ mm^3). A large size LCD and battery are settled in parallel with a 1 mm spacing and are connected with the main PCB via connectors. To maintain the thinness of the mobile devices, planar antenna is considered. Due to which, LCD is placed within the ground portion. Beyond the ground, antenna portions are overlapped by the LCD screen resulting in antenna performance deteriorated. By the trade-off between simplicity of the antenna structure and size of LCD, the MIMO antenna is placed on one top corner of the substrate which is off-display area while the large size LCD display is placed on the opposite side of the substrate. A camera and speaker are placed at the same side of the PCB (on the side of antenna elements). These components are near the antenna elements and deposed in the available space. All these components are assumed as perfect electric conductor (PEC) during simulations. The small metallic components, such as two buttons and one microphone, are also considered and are far from antenna elements. All these mobile components and antenna elements are covered with a 1 mm thick plastic box of dielectric constant 3.0 and conductivity of 0.02 S/m, which forms housing of the mobile phone. The effect of near-field mobile environment on S-parameters is shown in Figure 4(b). It is observed that a significant effect of the mobile environment is observed on the reflection and coupling S-parameters. It is interestingly noted that at lower frequency both impedance matching and isolation level are improved. This is due to the placement of the speaker near the antenna element which acts as a reflector for antenna elements. Due to the placement of speaker near the T-shaped protruded ground plane, electrical length of the T-shaped protruded ground increases by the capacitive coupling between T-shaped structure and speaker, and hence improved isolation is observed in the presence of mobile environment.

(a)   (b)
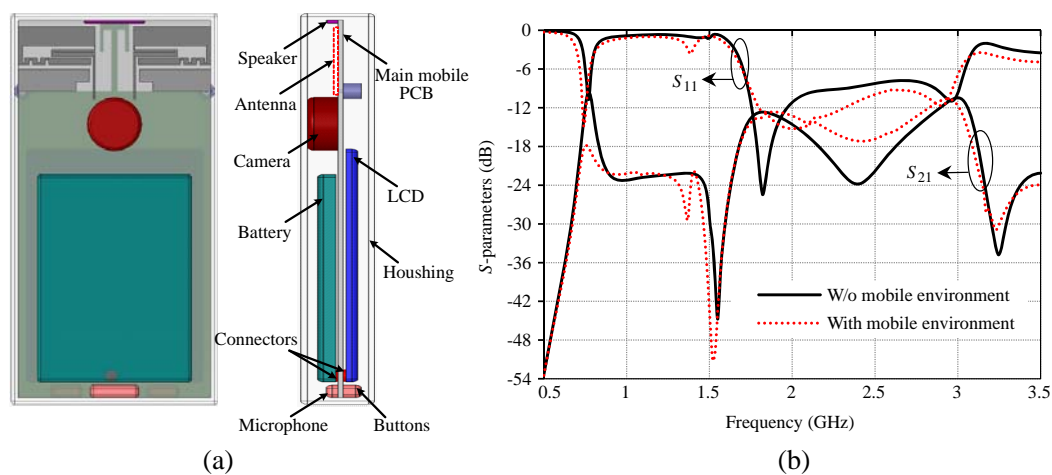
Figure 4. (a) Actual mobile environment with antenna elements and (b) effect of mobile environment on S-parameters.

3.2. Effect of User Proximity on Antenna Performances

The antenna performances are also studied in the presence of user proximity. In this section, the position of the whole antenna array and the user's body, i.e., head and hand (Talk mode), are in accordance with the CTIA revision 3.1 [20] by considering the antenna in a typical environment of multimedia mobile phone [mobile environment shown in Figure 4(a)] as shown in Figure 5(a). The dielectric properties of the human tissue used in this paper can be found in [20]. The effect of user proximity on the S-parameters is shown in Figure 5(b). It is observed that the presence of a user shows significant effect on the operating bands and isolation between ports. At lower frequency band, impedance matching gets improved, due to which bandwidth increases, whereas at higher frequency band the lower and upper cut-off frequencies are shifted towards the lower side without affecting the operating bands. Also, isolation between antenna ports gets improved, and it is well below $-13\,\mathrm{dB}$ throughout the operating bands.

Further, parameter considered in this study for evaluating the effect of a user is total radiated power (TRP) [20]. The calculated values of TRPs in free space and in user proximity are given in Table 1. It is ascertained that in the case of free space, TRPs of Ant. 1 and Ant. 2 are the same due to the uniform environment around the MIMO antenna elements. Due to the low reflection loss and high total efficiency, the TRPs in free space are high, i.e., more than $23\,\mathrm{dBm}$. When we implement the proposed antenna in a real scenario of mobile phone with user proximity, the TRPs decrease due to the large human body coverage around antenna elements but still better than $13\,\mathrm{dBm}$. The higher TRP can significantly improve the call performance of the handset in a weak signal area.

Since antennas are located on the top of the mobile circuit board which are in close vicinity of the human head, specific absorption rate (SAR) is of a main concern. The SAR is calculated for both the antennas individually and meets the criteria of American (FCC) and European standards [21]. The calculated values of SAR are given in Table 1. It is noticed that SAR for symmetrically placed MIMO elements is not equal due to the non-planar nature of the human head phantom.

(a)   (b)
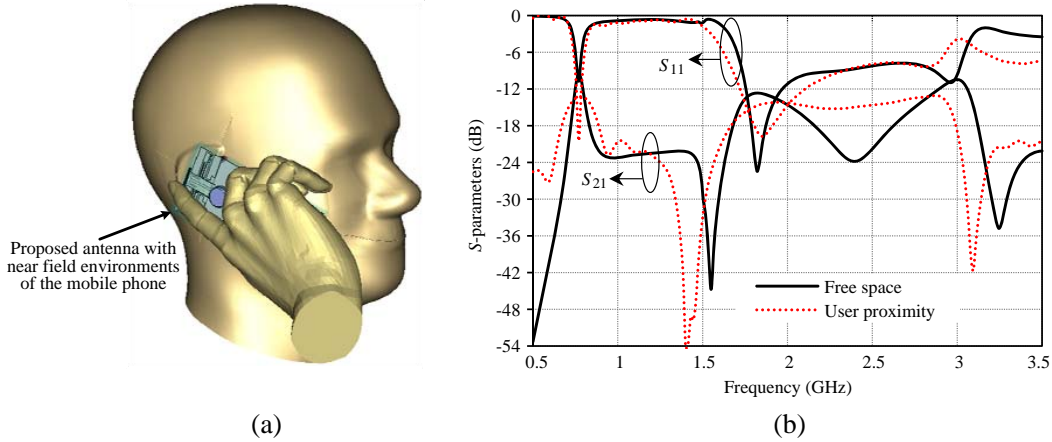
Figure 5. (a) User configuration with antenna, (b) effect of user proximity on S-parameters.

Table 1. Values of TRPs for the proposed antenna.

Freq. (GHz)	Total Radiated Power (TRP) (dBm)				Specific Absorption Rate (SAR)			
	Free space		User proximity		FCC (1 g)		European (10 g)	
	TRP1	TRP2	TRP1	TRP2	Ant. 1	Ant. 2	Ant. 1	Ant. 2
0.777	23.3	23.3	13.6	14.8	0.5	0.68	0.34	0.45
1.9	26.5	26.5	19.7	19.8	0.68	1.3	0.4	0.73
2.45	26	26	19	19.8	0.45	0.69	0.25	0.39
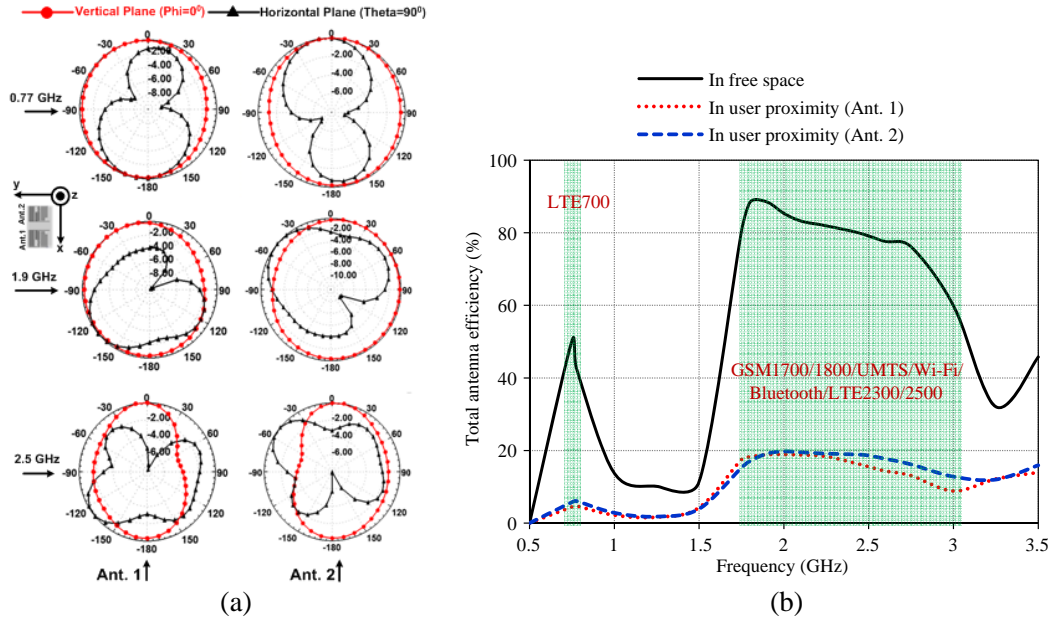
Figure 6. (a) Measured far field radiation patterns, (b) variation of total antenna efficiency with frequency.

3.3. Radiation Performances

The measured far-field radiation patterns of the proposed antenna array at different frequencies, i.e., 0.77 GHz, 1.9 GHz, and 2.5 GHz, are achieved by exciting the single port at a time and matched terminated to other port and are shown in Figure 6(a), which illustrates that the radiation patterns of the two elements point to complimentary spatial region which shows pattern diversity of the proposed antenna, and this property can provide low correlation and good antenna diversity in free space. Figure 6(b) shows the calculated total antenna efficiency by considering the reflection losses for the proposed antenna in free space as well as user proximity. Ant. 1 and Ant. 2 are identical and symmetrically placed on PCB of mobile circuit board. So total antenna efficiencies are almost the same for all antenna elements in free space, whereas in user proximity, they are not the same for all antenna elements because the user's hand placed asymmetrically between two ports of antenna elements. And also, it is observed that presence of a user will bring less efficiency than free space efficiency due to reflection losses by the human body. The total efficiency in the presence of user proximity is significantly low compared to the free space. However, this problem can be solved either by applying adaptive technique or the use of low loss material for antenna fabrication. In the adaptive technique, the best element can be chosen among the multiple antennas placed on the corners of the mobile circuit board.

3.4. Diversity Performances

The envelope correlation coefficient (ECC), mean effective gain (MEG), and effective diversity gain (EDG) are most important parameters for evaluating the diversity performances of the proposed antenna. The calculation of the diversity parameters are carried out by using CST MWS.

The ECC is calculated using far-field pattern data by considering lossy structure of the antenna system and uniform scattering environment. The ECC is calculated for the condition as given in [13], and ECCs in free space and in user proximity for the given condition are given in Table 2. It is observed that the values of ECC are well below within the allowable limit 0.5 for both the cases, i.e., free space and user proximity.

Further, MEG is calculated for the proposed antenna, which is defined by the ratio of the mean received power of antennas over a random route to the total mean incident power at the antenna elements [22], and calculation of MEG is similarly done as in [13]. The calculated values of MEGs are

Table 2. Diversity performance of the proposed MIMO antenna.

Frequency (GHz)	ECC (XPR = 0 dB)		Mean Effective Gain (dB) (XPR = 0 dB)				Effective Diversity Gain (1%) (dB)	
	Free space	User proximity	Free space		User proximity		Free space	User proximity
			MEG1	MEG2	MEG1	MEG2		
0.777	0.427	0.45	−6.8	−6.8	−17.2	−17.6	3.85	0.42
1.8	0.012	0.015	−5.3	−5.3	−12.1	−12.2	8.83	1.8
1.9	0.002	0.0042	−5.1	−5.1	−11.9	−12.2	8.84	1.88
2.1	0.0004	0.0015	−5.11	−5.11	−12.3	−11.7	8.31	1.88
2.5	0.0003	0.00056	−5.46	−5.46	−11.8	−12.3	7.9	1.54

given in Table 2, in free space and in user proximity. It is observed that MEGs are equal for both antennas in the case of free space while unequal in the case of user proximity. The presence of a user brings lower values of MEGs than free space due to unequal branch signals, but the ratios of MEGs are close to unity in both cases, which satisfy the equality criterion for the two antennas.

The next important diversity parameter is EDG. The apparent diversity gain which is based on selection combining w.r.t. 1% distribution level does not include the antenna efficiency. So we cannot achieve effectiveness of diversity capability without considering antenna efficiency. In view of this, here we calculate the effective diversity gain (EDG) as calculated in [23]. The calculated values of EDG in free space and in user proximity are given in Table 2. It is observed that EDG is lower in user proximity due to higher reflection losses and lower total antenna efficiency.

4. CONCLUSION

A compact planar MIMO antenna for LTE700/WWAN application is presented for a slim mobile handest. A protruded ground plane is used to enhance the isolation at higher frequency side. With the help of protruded ground plane, isolation at higher frequency band is achieved well below −10 dB. The proposed diversity antenna is also analysed in the presence of user proximity. The diversity parameters are calculated in free space as well as user proximity, and the results satisfy the diversity criterion. The calculated values of SAR on the human head phantom are well below the defined standard limit. The results of S-parameters, radiation patterns, antenna efficiency, ECC, MEG, and EDG are presented. All the results indicate that the proposed MIMO antenna system is a potential candidate for portable usages to combat multipath fading practical applications and promising for slim LTE/WWAN smart applications.

REFERENCES

1. Foschini, G. J. and M. J. Gans, "On limits of wireless communications in a fading environment when using multiple antennas," *Wireless Person. Commun.*, Vol. 6, No. 3, 311–335, 1998.
2. Lee, B., E. J. Harackiewicz, and H. Wi, "Closely mounted mobile handset MIMO antenna for LTE 13 band application," *IEEE Ant. and Wireless Propag. Lett.*, Vol. 13, 411–414, 2014.
3. Lee, J., Y.-K. Hong, S. Bae, G. S. Abo, W.-M. Seong, and G.-H. Kim, "Miniature long-term evolution (LTE) MIMO ferrite antenna," *IEEE Ant. and Wireless Propag. Lett.*, Vol. 11, 603–606, 2011.
4. Baek, J. and J. H. Choi, "The design of a LTE/MIMO antenna with high isolation using a decoupling network," *Microwave Opt. Tech. Lett.*, Vol. 56, No. 9, 2187–2191, 2014.
5. Yu, Y., G. Kim, J. Ji, and W. Seong, "A compact hybrid internal MIMO antenna for LTE application," *European Conference on Antennas and Propagation*, 1–2, Barcelona, Spain, Apr. 12–16, 2010.

6. Kim, B., Y. Park, H. Wi, M.-J. Park, Y. Choi, J. Lee, W. Jung, D. Kim, and B. Lee, "Isolation enhancement of USB dongle MIMO antenna in LTE700 band applications," *IEEE Ant. and Wireless Propag. Lett.*, Vol. 11, 961–964, 2012.

7. Park, G., M. Kim, T. Yang, J. Byun, and A. S. Kim, "The compact quad-band handset antenna for LTE700 MIMO application," *IEEE Antennas and Propagation Society International Symposium (APSURSI 2009)*, 1–4, Charleston, SC, Jun. 1–5, 2009.

8. Thomas, T., Y. V. B. Reddy, and K. Veeraswamy, "Small size printed antenna array for LTE/WWAN with LTE MIMO operation for mobile communication," *20th International Conference on Electronics and Communication Engineering*, 64–68, Banglore, India, May 2012.

9. Wong, K.-L., T.-W. Kang, and M.-F. Tu, "Internal mobile phone antenna array for LTE/WWAN and LTE MIMO operations," *Microwave Opt. Tech. Lett.*, Vol. 53, No. 7, 1569–1573, 2011.

10. Zhang, S., K. Zhao, Z. Ying, and S. He, "Adaptive quad-element multi-wideband antenna array for user-effective LTE MIMO mobile terminals," *IEEE Trans. on Antennas and Propag.*, Vol. 61, No. 8, 4275–4283, 2013.

11. Yang, S., T. Jiang, J. L.-W. Li, and Y.-L. Ban, "Internal low profile multi band MIMO antenna for WWAN/LTE mobile phone applications," *IEEE International Symposium Antennas and Propagation Society*, 522–523, Orlando, FL, Jul. 7–13, 2013.

12. Diallo, A., C. Luxey, P. Le thuc, R. Staraj, and G. Kossiavas, "Study and reduction of the mutual coupling between two mobile phone PIFAs operating in the DCS1800 and UMTS bands," *IEEE Trans. on Antennas Propag.*, Vol. 54, No. 11, 3063–3074, 2006.

13. Meshram, M. K., R. K. Animeh, A. T. Pimpale, and N. K. Nikolova, "A novel quad-band diversity antenna for LTE and Wi-Fi applications with high isolation," *IEEE Trans. on Antennas Propag.*, Vol. 60, No. 9, 4360–4371, 2012.

14. Chen, S. C., Y. S. Wang, and S. J. Chuang, "A decoupling technique for increasing the port isolation between two strongly coupled antennas," *IEEE Trans. on Antennas Propag.*, Vol. 56, No. 12, 3650–3658, 2008.

15. Zhang, S., S. N. Khan, and S. He, "Reducing mutual coupling for an extremely closely-packed tunable dual-element PIFA array through a resonant slot antenna formed in-between," *IEEE Trans. on Antennas Propag.*, Vol. 58, No. 8, 2771–2776, 2010.

16. Ban, Y.-L., Z. X. Chen, Z. Chen, K. Kang, and L. W. Li, "Decoupled closely-spaced hepta-band antenna array for WWAN/LTE smartphone applications," *IEEE Ant. and Wireless Propag. Lett.*, Vol. 13, 31–34, 2014.

17. Ban, Y.-L., S. Yang, Z. Chen, K. Kang, and J. L.-W. Li, "Decoupled planar WWAN antennas with T-shaped protruded ground for smartphone applications," *IEEE Ant. and Wireless Propag. Lett.*, Vol. 13, 483–486, 2014.

18. Ansoft High Frequency Structure Simulator (HFSS), Online Available: http://www.ansoft.com.

19. Computer Simulation Technology Microwave Studio (CST MWS), Online Available: http://www.cst.com.

20. CTIA, "CTIA certification test plan for mobile station over the air performance," Method of Measurement for Radiated RF Power and Receiver Performance, Washington, DC, Apr. 2005.

21. Durney, C. H., H. Massoudi, and M. F. Iskander, *Radiofrequency Radiation Dosimetry Handbook*, 4th Edition, Rep. USAF-SAM-TR-85-73, USAF School of Aerospace Medicine, Aerospace Medical Division (AFSC), Brook Air Force Base, Texas, Oct. 1986.

22. Taga, T., "Analysis for mean effective gain of mobile antennas in land mobile radio environments," *IEEE Trans. Veh. Technol.*, Vol. 39, 117–131, 1990.

23. Singh, H. S., B. R. Meruva, G. K. Pandey, P. K. Bharti, and M. K. Meshram, "Low mutual coupling between MIMO antennas by using two folded shorting strips," *Progress In Electromagnetics Research B*, Vol. 53, 205–221, 2013.